ACS OMEGA

http://pubs.acs.org/journal/acsodf

Article

Operando Monitoring of Oxygen Drop in Catalyst Layers Accompanied by a Water Increase in Running Proton Exchange Membrane Fuel Cells

Hiromichi Nishiyama and Junji Inukai*

Cite This: *ACS Omega* 2023, 8, 15318−15322

Read Online

ACCESS | Metrics & More | Article Recommendations | Supporting Information

ABSTRACT: Accurate understanding of internal phenomena and their feedback is intrinsically important for improving the performance and durability of proton exchange membrane fuel cells. The oxygen partial pressure ($p(O_2)$) at 10 μm from the cathode catalyst layer (CL) in the gas diffusion layer was measured by using an optical fiber with an oxygen-sensitive dye applied to the apex, when the current density was abruptly increased. $p(O_2)$ decreased with increasing current density at constant air utilization. This decrease in oxygen partial pressure is attributed to the increased amount of water at the CL at the cathode due to the oxygen reduction reaction and electro-osmotic drag, as previously proposed. A shortage of oxygen in the CL for 1 s was also detected by using this $p(O_2)$ monitoring. These results are consistent with the previous results obtained by *operando* time-resolved measurements of the water distribution in the electrolyte membranes of a running fuel cell.

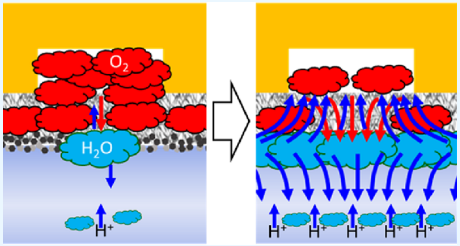

1. INTRODUCTION

Proton exchange membrane fuel cells (PEMFCs) are considered promising energy conversion devices due to their cleanliness and high efficiency. The operation of PEMFCs involves a number of chemical and physical phenomena, including electrochemical reactions and the transfer of heat, mass, and electron/ion charge; an accurate understanding of their internal reaction distribution is essentially important for improving the performance and durability of PEMFCs.

It has been shown that water management is critical to maximizing the performance and durability of PEMFCs.[1,2] To maintain good proton conductivity and performance, the inlet gas should be humidified to keep the membrane hydrated. On the other hand, excess liquid water can flood the catalyst layer (CL) and gas diffusion layer (GDL), as well as the gas flow channels, leading to a high mass transport resistance. To optimize the mode of operation, the behavior of the water or gas inside the fuel cell under operating conditions needs to be clarified. Hence, *operando* measurements have been carried out for liquid water in the membrane electrode assembly (MEA) and the gas flow channels of fuel cells by direct optical systems,[3−5] X-ray imaging,[6,7] neutron imaging,[8−10] and vibrational spectroscopy.[11−16] Recently, the oxygen partial pressure ($p(O_2)$) using oxygen-sensitive dye is measured during the power generation.[17−22] Higher special and temporal resolutions are being required for those *operando* measurements to understand the transient behavior in PEMFC especially used for automobile applications.

Previously, we reported on the water distribution in a transient state inside a proton exchange membrane (PEM) during a current density jump using time-resolved coherent anti-Stokes Raman scattering spectroscopy.[15,16] When the current density was suddenly increased, the cell voltage recovered in seconds after the initial rapid decrease. We found that the number of water molecules per sulfonic acid, λ, at the cathode surface of the PEM overshot in synchrony with the change in cell voltage (Figure S1 in the Supporting Information).[15] This sudden increase (overshoot) of water inside the membrane was lowered by the ejection of water to the CL or by the back diffusion of water into the membrane. Furthermore, the results of synchronous changes in λ and cell voltage suggested that the overshooting water discharged into the cathode CL temporarily lowered the amount of oxygen in the CL to be used for the power generation; the distributions of water and oxygen from the nanometer to micrometer scale were expected to have an effect on the transient power generation.

In this study, we now monitored $p(O_2)$ near the CL surface at the cathode during the current density jump. The decrease in $p(O_2)$ near the CL was clearly observed to follow the voltage drop. During this $p(O_2)$ change, the oxygen concentration in the CL was lowered as discussed in the previous study.[15]

Received: January 23, 2023
Accepted: April 5, 2023
Published: April 14, 2023

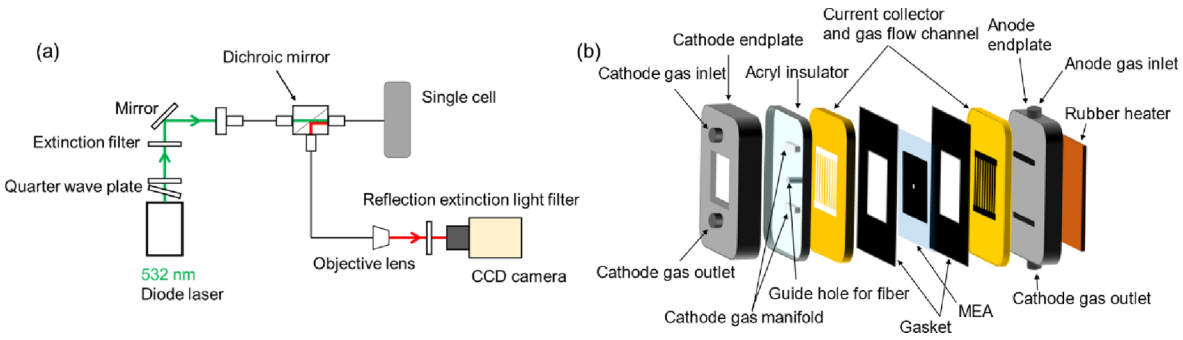

Figure 1. Schematic illustrations of $p(O_2)$ measurement system (a) and PEMFC designed for $p(O_2)$ measurement (b).

2. EXPERIMENTAL SECTION

2.1. Oxygen Monitoring in CL. Figure 1a shows a schematic representation of the $p(O_2)$ monitoring system reported previously.[21,22] An optical fiber was inserted into the cathode side of the cell, and a 532 nm diode laser light was irradiated onto the oxygen-sensitive dye film at the fiber apex. The excitation light and the emission at 650 nm were separated by a dichroic mirror, and the emission was detected by a CCD camera with a reflective filter for excitation light placed in front of the camera. In the center of the cathode side of the GDL, a pinhole 90 μm in diameter was created down to the CL.[12,14−16,22] An optical probe was inserted directly into a PEMFC through the hole.

The oxygen-sensitive dye, Pt(*II*)tetrakis-pentafluorophenyl-porphyrin (PtTFPP), was used as the oxygen sensor.[17−22] PtTFPP was mixed with poly(1-trimethylsilyl-1-propylene) (*poly*TMSP) and toluene, where the concentration of the dye solution was adjusted to 25 wt % for PtTFPP.

A single-mode optical fiber with a clad diameter of 125 μm and a core diameter of 10 μm was immersed in HF solution (pH = 2.9) and etched until the clad diameter became 50 μm. Afterward, the apex of the optical fiber was cut off flat perpendicular to the fiber axis. At the apex of the optical fiber, the oxygen-sensitive dye solution was used to form a dye film with a thickness of 2 μm.

The probe depth was controlled by a micrometer. For measuring the distance between the probe apex and the CL surface, a super luminescent diode light with a wavelength of 830 nm was introduced to the probe to obtain an interference light from the surfaces of the CL and the probe apex. The interference spectrum of reflection lights was Fourier-transformed to measure the distance with an accuracy of 1 μm.

2.2. Cell for Oxygen Monitoring. The structure of a cell with nine straight flow channels for $p(O_2)$ monitoring is shown in Figure 1b. The widths of the gas flow channels and the ribs and the depth of the gas flow channels were all 1 mm. On the cathode side of the stainless-steel end plate, a window is formed for the insertion of an optical probe. An acrylic insulator with a hole was inserted between the end plate and the current collector to position the probe. The hole for the optical probe was in the center of the active area under the central gas flow channel.

A catalyst-coated membrane (CCM) was prepared by spray coating both sides of the Nafion membrane (NRE211, E. I. du Pont de Nemours & Company, Inc.) with catalyst paste consisting of a Pt catalyst supported on carbon black (46.9 wt % Pt, Tanaka Kikinzoku Kogyo, Japan), pure water, ethanol, and 5 wt % Nafion ionomer (ion exchange capacity = 0.9 meq g^{-1}, DE521, E. I. du Pont de Nemours & Company, Inc.) with an ionomer/carbon volume ratio of 0.7, using a pulse whirl spray system (Nordson). The CCMs were dried in an oven at 60 °C for 12 h. The thickness of the CL was approximately 7 μm. The active area was 20 mm × 20 mm.

For the MEA, a CCM and GDLs with microporous layers (MPLs) (SIGRACET 29 BC, SGL Carbon Group Co., Ltd.) were sandwiched. The tightening pressure of the cell was 2.4 kN.

2.3. $p(O_2)$ Measurement. For the power generation, a test bench (As-510-340PE, NF Circuit Design Block Co.) was used. The cathode and anode gases were supplied as parallel flows. The cell temperature was set at 80 °C and the relative humidity (RH) at 80%. An optical probe was inserted and placed 10 μm from the CL. To obtain a calibration curve for $p(O_2)$, a mixture of N_2 and air gases of different concentrations was supplied to both the anode and cathode at 500 mL min^{-1} for 10 min. At each gas mixture rate, the emission was measured five times with a CCD camera with an exposure time of 400 ms and averaged. The emission intensity of the oxygen-sensitive dye degraded linearly with laser irradiation at approximately 0.06% s^{-1}. To obtain $p(O_2)$ using this dye, the degradation factor was complemented after the emission data had been acquired. The calibration curve is shown in Figure 2. Using this calibration curve and the Stern−Volmer

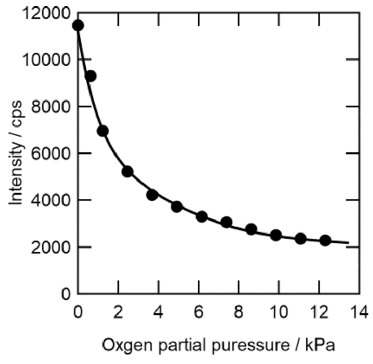

Figure 2. Calibration curve for oxygen using an oxygen-sensitive dye at the fiber apex.

equation, $p(O_2)$ was determined.[24] We have previously studied the influence of the water vapor pressure on the emission from the dye film and made clear that the water vapor partial pressure had no influence on monitoring $p(O_2)$.[17]

The Stern−Volmer equation is formulated as in eq 1:

$$\frac{I_0}{I} = k\,\tau\,p(O_2) \quad (1)$$

https://doi.org/10.1021/acsomega.3c00461
ACS Omega 2023, 8, 15318−15322

where I_0 is the intensity without a quencher, I is the intensity with a quencher, k is the quencher rate coefficient, and τ is the lifetime of the emissive excited without a quencher present.

The cell was operated at 80 °C and 80% RH. The power generation at 0.1 A cm^{-2} was continued for 20 min, and the current density was jumped (at t = 0 s in to either 0.3, 0.5, or 0.7 A cm^{-2}). The emission from the oxygen-sensitive dye and the cell voltage were recorded every 400 and 50 ms, respectively. The effect of the 90 μm hole created inside the GDL and the insertion of a 50 μm optical fiber on $p(O_2)$ at the apex was estimated to be less than 1% by a fluid-flow computation using mixtures of air and water vapor under the operational conditions.[22] During the continuous irradiation of laser light onto the dye film, the emission intensity degraded linearly with laser irradiation at approximately 0.06% s^{-1}, which was easily corrected. In this method, the error in the experiments was thus estimated to be ±2%.[22] Therefore, the fluctuations observed in the following Figure 3b are not experimental errors.

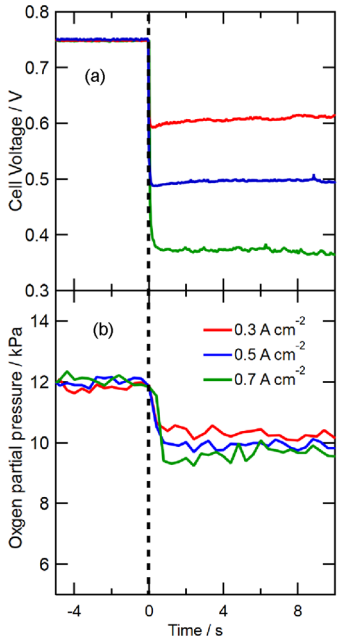

Figure 3. Transient values of cell voltage (a) and $p(O_2)$ (b). Current density was jumped from 0.1 to 0.3 (red), 0.5 (blue), and 0.7 A cm^{-2} (green) at 0 s. Temperature = 80 °C, RH = 80%. H_2 and air utilization = 40 and 70%, respectively.

The degree of pressure drop within the cell can impact the oxygen concentration. To understand the potential drops along the gas channels, we previously investigated the pressure drop using a single cell with straight channels by the combination of the visualization of $p(O_2)$ and numerical simulations.[23] Under the ambient pressure, the effect of the potential drop along the straight flow channel was negligibly small.

To summarize, experimental parameters are listed in Table 1.

Table 1. Parameters for $p(O_2)$ Monitoring

optical fiber	single mode, clad diameter 50 μm, core diameter 10 μm
distance from CL surface	10 μm
oxygen sensitive dye	PtTFPP + polyTMSP
laser irradiation wavelength	532 nm
dye emission wavelength	650 nm
active area	20 mm × 20 mm
gas flow channel	9 channels, width and depth 1 mm
membrane	Nafion NRE211
catalyst	Pt on carbon black
GDL	SIGRACET 29 BC
cell temperature	80 °C
gas humidity	80% RH
current density	0.1, 0.3, 0.5, 0.7 A cm^{-2}

3. RESULTS AND DISCUSSION

After the current density was kept at 0.1 A cm^{-2} for 20 min, it was abruptly jumped to 0.3, 0.5, or 0.7 A cm^{-2}. The moment of the current density jump was defined as t = 0 as in Figure 3. Figure 3a,b shows the time variation of cell voltage and $p(O_2)$ from t = −5 to 10 s, respectively. At 0.1 A cm^{-2}, the cell voltage showed a constant value of approximately 0.745 V, which dropped after the current density jump. In our previous study, clear voltage oscillations were observed using the cell without MPLs at the GDLs.[22] In this study with an MPL, the discharge of water was prompted from the CL, and the oscillations in cell voltage were not observed. From 30 s before the current density jump, the gas flow in the cell was increased according to the set current value after the current density jump; thus, the oxygen utilization at 0.1 A cm^{-2} was set to 13.3, 8.0, and 5.7% for current density jumps to 0.3, 0.5, and 0.7 A cm^{-2}, respectively. After the current density jumps, the utilization of oxygen was set at 40% and that of hydrogen at 70% at all current densities. For all current density jumps, transitions in voltage were observed on the order of 10 s. This is in agreement with numerical simulation results previously reported.[25,26]

After the current density jump from 0.1 to 0.3 cm^{-2}, the voltage immediately dropped from 0.745 to 0.598 V and recovered slowly to a steady value of 0.610 V after 5.0 s (Figure 3). This behavior of the cell voltage upon the current density jump was similar to that reported previously (Figure S1).[15] After the current density jump, $p(O_2)$ decreased to 10.3 kPa over 1 s and slowly kept decreasing to 10.0 kPa. The decrease in $p(O_2)$ at 1 s after the current density jump is considered to be due to the increased oxygen utilization as well as water that has increased at the cathode CL and discharged into the gas flow channel.[27] Therefore, interestingly, for seconds after the current density jump, the cell voltage increased whereas $p(O_2)$ decreased. This slow decrease in $p(O_2)$ near the CL surface may be due to an increase in gas diffusivity at the CL/gas interface due to the gradual decrease of water after the overshoot of the water content in the membrane. The influence of the gas diffusivity of the interface on $p(O_2)$ near the CL was previously reported (Figure S2b).[22] The voltage increased accordingly.

Because of flooding, the highest current density obtained was 0.7 A cm^{-2}. After the current density jump from 0.1 to 0.7 A cm^{-2}, the voltage immediately dropped to 0.390 V and slowly kept decreasing to 0.361 V probably due to continuing partial flooding. After the current density jump, $p(O_2)$ decreased to 9.3 kPa over 1 s and slowly increased to 9.7 kPa in contrast to the decrease in cell voltage. The amount of water in the CL was expected to slowly increase accompanied by the decrease in the gas diffusivity of the CL/gas interface, corresponding to the increase in $p(O_2)$ at 10 μm from the CL

https://doi.org/10.1021/acsomega.3c00461
ACS Omega 2023, 8, 15318−15322

(Figure S2a).[22] The decrease in the cell voltage is also explained by the decrease in the gas diffusivity in the CL.

In the jump to 0.5 A cm^{-2}, the cell voltage and $p(O_2)$ behaved between in jumps to 0.3 and to 0.7 A cm^{-2}. Namely, the cell voltage sharply decreased to 0.489 V, and the value was almost constant for seconds. $p(O_2)$ decreased to 9.9 kPa over 1 s and almost constant. Upon the jump to 0.5 A cm^{-2}, the amount of water in the CL was expected to increase in the CL and was kept nearly constant for seconds.

After the current density jump, it took approximately 1 s for $p(O_2)$ to be at the lower stages. Upon the current density jump, the consumption of oxygen at the CL simultaneously increased. On the other hand, the diffusion of oxygen from the gas flow channel to the CL was not spontaneous, taking 1 s to be stabilized possibly because of the change in water content in the CL. The values of $p(O_2)$ were decreased by 1.6, 2.1, and 2.3 kPa when the current density jumped from 0.1 to 0.3, 0.5, and 0.7 A cm^{-2}, respectively, at the same oxygen utilization of 40%. Therefore, the different $p(O_2)$ decreases at different current density jumps can be considered to originate from the different amounts of water produced by the ORR and those transported from the anode by the electro-osmotic drag. Previously, upon current density jumps, the number of water molecules per sulfonated group, λ, at the cathode surface of the PEM was found to overshoot in synchrony with the cell voltage, which led to the consideration that the increased water at the cathode temporarily shortened oxygen in the cathode CL.[15] The temporary shortage of oxygen in the CL by the increase of water was clearly reflected by the lowering of $p(O_2)$ taking 1 s after the current density jump (Figure 3).

Interestingly, for the current density jump to 0.3 A cm^{-2}, the cell voltage recovered after the initial voltage drop and $p(O_2)$ decreased, whereas, for the current density jump to 0.7 A cm^{-2}, the cell voltage decreased progressively after the initial voltage drop and $p(O_2)$ increased. The decrease in cell voltage after the current density jump to 0.7 A cm^{-2} can be explained by the lowered diffusivity of oxygen in the CL due to the water produced by the ORR.

These results were obtained only at a single point in the center of an MEA of 20 mm × 20 mm at the distance of 10 μm from the CL and do not imply a water behavior over the entire cell. Further experiments at various locations and under various conditions are needed to fulfill the reaction distributions throughout the cell for higher stability and durability.

4. CONCLUSIONS

$p(O_2)$ at the location 10 μm from the CL at the current density jump was measured using an optical fiber and an oxygen-sensitive dye during power generation of polymer electrolyte fuel cells at 80 °C and 80% RH. $p(O_2)$ decreased with the current density jump. A temporary shortage of oxygen in the CL was observed by the slower change of $p(O_2)$ in 1 s at the location 10 μm from the CL. During flooding, $p(O_2)$ at 10 μm from the CL increased, contrary to the decrease in cell voltage, probably because the diffusion of oxygen was inhibited by increasing water in the CL.[22]

Transient behavior in a PEMFC is reflected by the transient distributions of physical/chemical parameters inside. Further *operando* measurements coupled with numerical simulations are required.

ASSOCIATED CONTENT

Supporting Information

The Supporting Information is available free of charge at https://pubs.acs.org/doi/10.1021/acsomega.3c00461.

Transient values of cell voltage, ohmic resistance and λ; current density jump; oxygen partial pressure; GDL and MPL; gas flow channels and ribs (PDF)

AUTHOR INFORMATION

Corresponding Author

Junji Inukai − *Hydrogen and Fuel Cell Nanomaterials Center, University of Yamanashi, Kofu, Yamanashi 400-0021, Japan; Clean Energy Research Center, University of Yamanashi, Kofu, Yamanashi 400-8510, Japan;* orcid.org/0000-0002-7819-842X; Phone: +81 55 220 8185; Email: jinukai@yamanashi.ac.jp; Fax: +81 55 220 8185

Author

Hiromichi Nishiyama − *Hydrogen and Fuel Cell Nanomaterials Center, University of Yamanashi, Kofu, Yamanashi 400-0021, Japan;* Present Address: LIB Technical Center, GS Yuasa International Ltd., 780-1, Hachiya, Ritto, Shiga 520-3021, Japan (H.N.); orcid.org/0000-0003-0439-0002

Complete contact information is available at: https://pubs.acs.org/10.1021/acsomega.3c00461

Notes

The authors declare no competing financial interest.

ACKNOWLEDGMENTS

This work was performed under SPer-FC, ECCEED'30-FC, and ECCEED-GDL projects of the New Energy and Industrial Technology Development Organization (NEDO), Japan, and partly supported by the Ministry of Education, Culture, Sports, Science and Technology (MEXT), Japan, the Heiwa Nakajima Foundation, and the Yanmar Environmental Sustainability Support Association.

REFERENCES

(1) Le Canut, J.-M.; Abouatallah, R. M.; Harrington, D. A. Detection of Membrane Drying, Fuel Cell Flooding, and Anode Catalyst Poisoning on Pemfc Stacks by Electrochemical Impedance Spectroscopy. *J. Electrochem. Soc.* **2006**, *153*, A857.

(2) Van Nguyen, T.; Knobbe, M. W. A Liquid Water Management Strategy for PEM Fuel Cell Stacks. *J. Power Sources* **2003**, *114*, 70−79.

(3) Tüber, K.; Pócza, D.; Hebling, C. Visualization of Water Buildup in the Cathode of a Transparent PEM Fuel Cell. *J. Power Sources* **2003**, *124*, 403−414.

(4) Takada, K.; Ishigami, Y.; Hirakata, S.; Uchida, M.; Nagumo, Y.; Inukai, J.; Nishide, H.; Watanabe, M. Imaging of Water Droplets Formed During PEFC Operation on GDLs with Different Pore Sizes. *Electrochemistry* **2011**, *79*, 388−391.

(5) Sugiura, K.; Shiramizu, T.; Yamauchi, T.; Yamauchi, M.; Matsuzaki, S.; Kada, N.; Itoh, Y. Development of a High Performance Separator for PEFC by Visualization Technique. *ECS Trans.* **2008**, *12*, 131−138.

(6) Csoklich, C.; Steim, R.; Marone, F.; Schmidt, T. J.; Büchi, F. N. Gas Diffusion Layers with Deterministic Structure for High Performance Polymer Electrolyte Fuel Cells. *ACS Appl. Mater. Interfaces* **2021**, *13*, 9908−9918.

(7) White, R. T.; Orfino, F. P.; Hannach, M. E.; Luo, O.; Dutta, M.; Young, A. P.; Kjeang, E. 3D Printed Flow Field and Fixture for

Visualization of Water Distribution in Fuel Cells by X-Ray Computed Tomography. *J. Electrochem. Soc.* **2016**, *163*, F1337−F1343.
(8) Ludlow, D. J.; Calebrese, C. M.; Yu, S. H.; Dannehy, C. S.; Jacobson, D. L.; Hussey, D. S.; Arif, M.; Jensen, M. K.; Eisman, G. A. PEM Fuel Cell Membrane Hydration Measurement by Neutron Imaging. *J. Power Sources* **2006**, *162*, 271−278.
(9) Nasu, M.; et al. Neutron Imaging of Generated Water inside Polymer Electrolyte Fuel Cell Using Newly-Developed Gas Diffusion Layer with Gas Flow Channels During Power Generation. *J. Power Sources* **2022**, *530*, No. 231251.
(10) Mishler, J.; Wang, Y.; Mukundan, R.; Spendelow, J.; Hussey, D. S.; Jacobson, D. L.; Borup, R. L. Probing the Water Content in Polymer Electrolyte Fuel Cells Using Neutron Radiography. *Electrochim. Acta* **2012**, *75*, 1−10.
(11) Tabuchi, Y.; Ito, R.; Tsushima, S.; Hirai, S. Analysis of in situ Water Transport in Nafion® by Confocal Micro-Raman Spectroscopy. *J. Power Sources* **2011**, *196*, 652−658.
(12) Hara, M.; Inukai, J.; Miyatake, K.; Uchida, H.; Watanabe, M. Temperature Dependence of the Water Distribution inside a Nafion Membrane in an Operating Polymer Electrolyte Fuel Cell A Micro-Raman Study. *Electrochim. Acta* **2011**, *58*, 449−455.
(13) Peng, Z.; Huguet, P.; Deabate, S.; Morin, A.; Sutor, A. K. Depth-Resolved Micro-Raman Spectroscopy of Tri-Layer PFSA Membrane for PEM Fuel Cells: How to Obtain Reliable Inner Water Contents. *J. Raman Spectrosc.* **2013**, *44*, 321−328.
(14) Nishiyama, H.; Takamuku, S.; Oshikawa, K.; Lacher, S.; Iiyama, A.; Inukai, J. Chemical States of Water Molecules Distributed inside a Proton Exchange Membrane of a Running Fuel Cell Studied by *Operando* Coherent anti-Stokes Raman Scattering Spectroscopy. *J. Phys. Chem. C* **2020**, *124*, 9703−9711.
(15) Nishiyama, H.; Takamuku, S.; Iiyama, A.; Inukai, J. Dynamic Distribution of Chemical States of Water inside a Nafion Membrane in a Running Fuel Cell Monitored by *Operando* Time-Resolved CARS Spectroscopy. *J. Phys. Chem. C* **2020**, *124*, 19508−19513.
(16) Nishiyama, H.; Iiyama, A.; Inukai, J. The Distribution and Diffusion Coefficient of Water inside a Nafion® Membrane in a Running Fuel Cell under Transient Conditions Analyzed by *Operando* Time-Resolved CARS Spectroscopy. *J. Power Sources Adv.* **2022**, *13*, No. 100080.
(17) Inukai, J.; Miyatake, K.; Takada, K.; Watanabe, M.; Hyakutake, T.; Nishide, H.; Nagumo, Y.; Watanabe, M.; Aoki, M.; Takano, H. Direct Visualization of Oxygen Distribution in Operating Fuel Cells. *Angew. Chem. Int.* **2008**, *47*, 2792−2795.
(18) Takada, K.; Ishigami, Y.; Inukai, J.; Nagumo, Y.; Takano, H.; Nishide, H.; Watanabe, M. Simultaneous Visualization of Oxygen Distribution and Water Blockages in an Operating Triple-Serpentine Polymer Electrolyte Fuel Cell. *J. Power Sources* **2011**, *196*, 2635−2639.
(19) Takanohashi, K.; Suga, T.; Uchida, M.; Ueda, T.; Nagumo, Y.; Inukai, J.; Nishide, H.; Watanabe, M. Simultaneous Visualization of Oxygen Partial Pressure, Current Density, and Water Droplets in Serpentine Fuel Cell During Power Generation for Understanding Reaction Distributions. *J. Power Sources* **2017**, *343*, 135−141.
(20) Kakizawa, Y.; Schreiber, C. L.; Takamuku, S.; Uchida, M.; Iiyama, A.; Inukai, J. Visualization of the Oxygen Partial Pressure in a Proton Exchange Membrane Fuel Cell During Cell Operation with Low Oxygen Concentrations. *J. Power Sources* **2021**, *483*, No. 229193.
(21) Inukai, J. Development and Commercialization of Oxygen Concentration Monitor inside Fuel Cell Using Microprobes. *J. Surf. Finish. Soc. Jpn.* **2020**, *71*, 6−9.
(22) Kakizawa, Y.; et al. Oscillation Mechanism in Polymer Electrolyte Membrane Fuel Cell Studied by *Operando* Monitoring of Oxygen Partial Pressure Using Optical Probes. *J. Surf. Finish. Soc. Jpn.* **2021**, *72*, 230−237.
(23) Nagase, K.; Motegi, H.; Yoneda, M.; Nagumo, Y.; Suga, T.; Uchida, M.; Inukai, J.; Nishide, H.; Watanabe, M. Visualization of Oxygen Partial Pressure and Numerical Simulation of a Running Polymer Electrolyte Fuel Cell with Straight Flow Channels to Elucidate Reaction Distributions. *ChemElectroChem* **2015**, *2*, 1495−1501.
(24) Lakowicz, J. R. *Topics in Fluorescence Spectroscopy*; Springer, 1991.
(25) Wang, Y.; Wang, C.-Y. Transient Analysis of Polymer Electrolyte Fuel Cells. *Electrochim. Acta* **2005**, *50*, 1307−1315.
(26) Wang, Y.; Wang, C.-Y. Dynamics of Polymer Electrolyte Fuel Cells Undergoing Load Changes. *Electrochim. Acta* **2006**, *51*, 3924−3933.
(27) Wang, Y.; Wang, C.-Y. Two-Phase Transients of Polymer Electrolyte Fuel Cells. *J. Electrochem. Soc.* **2007**, *154*, B636.

https://doi.org/10.1021/acsomega.3c00461
ACS Omega 2023, 8, 15318−15322